Available online at www.sciencedirect.com
SCIENCE DIRECT
ELSEVIER
Ultramicroscopy 106 (2006) 561–573
ultramicroscopy
www.elsevier.com/locate/ultramic

Determination of chromium valence over the range Cr(0)–Cr(VI) by electron energy loss spectroscopy

Tyrone L. Daulton[a,*], Brenda J. Little[b]

[a]*Marine Geosciences Division, Naval Research Laboratory, Stennis Space Center, MS 39529, USA*
[b]*Oceanography Division, Naval Research Laboratory, Stennis Space Center, MS 39529, USA*

Received 9 August 2005; received in revised form 31 January 2006; accepted 10 February 2006

Abstract

Chromium is a redox active 3d transition metal with a wide range of valences (−2 to +6) that control the geochemistry and toxicity of the element. Therefore, techniques that measure Cr valence are important bio/geochemical tools. Until now, all established methods to determine Cr valence were bulk techniques with many specific to a single, or at best, only a few oxidation state(s). We report an electron energy loss spectroscopy (EELS) technique along with an extensive suite of affined reference spectra that together, unlike other methods, can determine Cr valence (or at least constrain the possible valences) at high-spatial resolution (tens-of-nanometer scale) across a wide valence range, Cr(0)–Cr(VI). Fine structure of Cr-$L_{2,3}$ edges was parametrized by measurement of the chemical shift of the L_3 edge and the ratio of integrated intensity under the L_3 and L_2 edges. These two parameterizations were correlated to Cr valence and also the d^n orbital configuration which has a large influence on L-edge fine structure. We demonstrate that it is not possible to unambiguously determine Cr valence from only one fine-structure parameterization which is the method employed to determine metal valence by nearly all previous EELS studies. Rather, multiple fine-structure parameterizations must be used together if the full range of possible Cr valences is considered. However even with two parameterizations, there are limitations. For example, distinguishing Cr(IV) from Cr(III) is problematic and it may be difficult to distinguish low-spin Cr(II) from Cr(III). Nevertheless, when Cr is known to be divalent, low- and high-spin d^n orbital configurations can be readily distinguished.
Published by Elsevier B.V.

PACS: 79.20.Uv; 68.37.Lp; 82.80.Dx; 82.80.Pv

Keywords: Electron energy loss spectroscopy; Chromium valence determination; $L_{2,3}$-adsorption edges; Transmission electron microscopy

1. Introduction

Chromium occurs in a variety of minerals [1] found in meteorites of all petrographic classes [2], lunar basalts [3], Martian rocks and the Earth, recording valuable information concerning geochemical conditions of mineralization and subsequent alteration. For example, many Cr-bearing minerals crystallize from basaltic magma where the valence of the mineralized Cr as well as the partitioning of Cr between solids/liquid and metal/silicates is dependent on oxygen fugacity and temperature [3–5]. Although recently challenged [6], the similar depletions of Cr estimated for the Earth and the Moon (based on inferred Cr partitioning coefficients) with respect to the most primitive chronditic meteorites have been considered the strongest evidence for a terrestrial origin of the Moon [7]. In the terrestrial crust, Cr is a common constituent of ultramafic rocks, such as peridotite and their serpentines, e.g. chromite $(Fe,Mg)(Cr,Al,Fe)_2O_4$ [8]. Natural weathering of Cr bearing minerals [9] and fallout of volcanic ash release Cr into the terrestrial environment. Furthermore, Cr compounds are widely used in numerous industrial processes [10] that can discharge Cr complexes in soils/sediments and surface/

*Corresponding author. Present address. Center for Materials Innovation, Washington University in St. Louis, St. Louis, MO 63130, USA. Tel.: +1 314 935 4537; fax: +1 314 935 6644.
E-mail address: tdaulton@physics.wustl.edu (T.L. Daulton).

0304-3991/$ - see front matter Published by Elsevier B.V.
doi:10.1016/j.ultramic.2006.02.005

ground waters, as well as the atmosphere in the form of aerosols. The geochemistry and toxicity of Cr in the environment are largely controlled by the valence of this redox active 3d transition metal. Chromium valence can be altered by microbes [11–13], green algae [14], higher plants [14,15] and mineral surfaces [16–19]. Therefore, techniques that determine Cr oxidation state are important bio/geochemical tools.

Chromium has a wide range (−2 to +6, in rare cases −4 and −3 are reported) of possible oxidation states [20–24]. Of these, only two, trivalent Cr(III) and hexavalent Cr(VI), are stable in the majority of terrestrial surface and aqueous environments [25,26]. Thermodynamic calculations predict Cr(VI) is most stable form in oxygenated aqueous solutions (0.15×10^{-4}–5.0×10^{-4} mol/L dissolved O_2) for pH $\geqslant 7$ while for pH $\leqslant 6$ Cr(III) is the most stable form [27]. Further, nearly all mineralized Cr in the terrestrial crust is trivalent presumably in disequilibrium with the atmosphere because of kinetic barriers [28].

Valence of Cr strongly affects many biogeochemical properties of Cr complexes including solubility, adsorption affinity and toxicity. All Cr(VI) species are soluble oxides, and the three main Cr(VI) species in solution are highly soluble chromate (CrO_4^{2-}), hydrochromate ($HCrO_4^-$) and dichromate ($Cr_2O_7^{2-}$) anions [29,30]. Hexavalent (as well as pentavalent) Cr species are strong oxidants which act as carcinogens, mutagens and teratogens in biological systems (for reviews, see Refs. [25,31,32]). The structural similarly of chromate anions (dominant Cr(VI) species at pH < 6.1, [30]) to biologically important inorganic anions, such as SO_4^{2-} and PO_4^{3-}, is likely responsible for their ability to readily transverse cell membranes, via the sulfate transport system, and be incorporated into cells (for reviews, see Refs. [32,33]). In contrast, most water soluble Cr(III) species do not occur naturally and are unstable in the environment [25]. Only under very acidic (pH $\leqslant 5$) or very basic (14 $\leqslant$ pH) conditions will Cr(III) exhibit solubility above 10 μM concentration [34,35]. In solution, Cr(III) exists as the cations $^{l}Cr^{3+}(aq)$ and hydroxo complexes $Cr_m(OH)_n^{(3m-n)+}$ [34]. However, $^{l}Cr^{3+}(aq)$ and $Cr(OH)_n^{(3-n)}$ complexes can be removed significantly from solution through adsorption by organic carbon [36] and mineral surfaces [37–39]. Therefore, Cr(III) species have low toxicity, in part, because their bioavailability is limited by low solubility and the tendency to form strong complexes with organics and hydroxo complexes. In contrast, the high mobility (solubility), bioavailability (uptake) and toxicity of Cr(VI) make it a particular environmental concern.

Geochemical and microbiological processes of Cr oxidation/reduction can drive both precipitation–dissolution and ion absorption–desorption reactions in the environment. The study of these reactions as well as the study of the Cr redox processes themselves has been hindered by the lack of an analytical technique that can determine the oxidation state of Cr at high-spatial resolution. For instance, little is known about the redox intermediates. Redox intermediates of Cr are unstable with intermediate valence between the valences of the stable end member forms. Previous studies have suggested the existence of several Cr redox intermediates in the reduction of Cr(VI):Cr(V) [14,40–45] and Cr(IV) [46]. To fully understand the geochemistry of Cr in the environment it is necessary to identify redox intermediates and the associated pathways involved in the interconversion of the different forms of Cr. This requires a technique that can determine Cr valence over a wide range of valences.

Nearly all of the established methods to determine Cr valence are bulk techniques and many are specific to only a few oxidation states. The most widely used method for measuring Cr in the environment is the diphenylcarbazide colorimetric method that is assumed specific to Cr(VI) [25,47]. However, Cr(V), a possible redox intermediate in reduction of Cr(VI) to Cr(III) by bacteria [42,44,45] and green algae [14], reacts with diphenylcarbazide to form stoichiometric oxidation products that exhibit similar photon absorbence as reaction products of Cr(VI) [48]. Spectroscopic methods using element specific detectors combined with chromatographic separations have been used to detect a limited number of valences of select metals (e.g., Cr(III) and Cr(VI)). Such methods include: flame (F)- and electrothermal (ET)- atomic adsorption spectrometry (AAS); direct current plasma (DCP)- and inductively coupled plasma (ICP)- atomic emission spectrometry (AES); inductively coupled plasma mass spectroscopy (ICP-MS); UV–vis spectrometry and thermal lens spectrometry (TLS) (for a review see Ref. [49]). Furthermore, valence of 3d or 4d transition metals can be analyzed by X-ray fluorescence spectrometry (XRS) [50], X-ray photoemission spectroscopy (XPS) [51], X-ray absorption spectroscopy (XAS) [3,52], electron paramagnetic resonance (EPR) (also known as electron spin resonance (ESR)) spectroscopy [42,53,54], high-field (HF)- EPR spectroscopy (for integer-spin "EPR-silent" transition metals) [55], Auger electron spectroscopy (AES) [56], and Mössbauer spectroscopy [57]. However, it has been reported that Mössbauer spectroscopy cannot be applied to Cr because of the lack of suitable Cr isotopes for measurement [58]. None of these techniques can determine metal valence at the submicron level in the proper biological/petrological context necessary for understanding the environmental processes of Cr reduction/oxidation.

Electron energy loss spectroscopy (EELS) using transmission electron microscopy (TEM) is capable of determining valence of metals at high-spatial (nm) resolution (e.g. see Refs. [59–62]). Further, it has been demonstrated that electron energy-filtered TEM imaging can produce valence specific maps of metals [63–65]. Determination of oxidation state by EELS (as well as XPS and XAS) is accomplished by analyzing valence-induced differences in the fine structure of absorption edges through the comparison of unknowns to standards of known oxidation state. Absorption edges result from excited electron transitions to unoccupied states such as in the valence band of a metal. For EELS valence determination of transition metals, the most often used absorption edges are the well-separated L_2 and L_3 (or

collectively $L_{2,3}$), however overlapping M_2 and M_3 (collectively $M_{2,3}$) edges [66] have been recently utilized. Valence of rare-earth and actinide metals have been determined by EELS using the well-separated M_4 and M_5 edges [61,67–69].

The $L_{2,3}$ absorption edges arise from transitions to unoccupied d levels from two spin–orbit split levels, $2p_{1/2}$ level (producing the L_2 edge) and the $2p_{3/2}$ level (producing the L_3 edge). Valence of a transition metal is related to the number of holes in the d level (i.e. the $3d^n$ or $4d^n$ configuration). For example with bound atoms, the ground state configuration of Cr(0) is considered [Ar] $3d^6$ ($[Ar]3d^54s^1$ corresponds to an isolated atom) while the other-shell configuration for Cr(III) is $3d^3$ and Cr(VI) is $3d^0$ (empty d orbital). Valence can affect the position, shape and relative intensity of $L_{2,3}$ absorption edges. Techniques previously used to determine mixed/single valence states involve analysis of either (a) the position of the $L_{2,3}$ absorption edges [60], (b) the ratio of the integrated-peak intensity $I(L_3)/I(L_2)$ (henceforth abbreviated L_3/L_2) [60,62], (c) least-squares fit of calculated or measured standard spectra to the shape of $L_{2,3}$ absorption edges [70,71].

There have only been a few EELS studies of the dependence of Cr-$L_{2,3}$ edge fine structure on Cr oxidation state. No one EELS study has systematically examined Cr-$L_{2,3}$ edge fine structure from a wide range of valences under identical instrumental conditions. For Cr valence determination using EELS, we have previously proposed a valence correlation technique using two parameterizations of the Cr-$L_{2,3}$ edge fine structure [72] and applied the nascent technique to study microbial reduction of Cr(VI) [46,73,74]. However, a very limited number of Cr-valence reference standards were used, severely limiting the EELS valence determination to only stable forms, Cr(VI) or Cr(III). Here we apply the two-parameterization valence-correlation technique on a greatly expanded set of Cr-valence reference standards that span Cr(0) to Cr(VI). Methods of data collection and processing were refined, resulting in far reduced scatter in the fine-structure parameterizations. With the new reference data, we demonstrate that the spin state of the 3d orbital has a large effect on Cr-$L_{2,3}$ edge fine structure and must be taken into consideration for Cr valence determination. We further demonstrate that because other factors in addition to valence can influence Cr-$L_{2,3}$ edge fine structure, multiple parameterizations of the fine structure must be used together to determine valence, if the full range of Cr valences is considered. Although there are still limitations using two parameterizations, the correlation technique is nonetheless powerful and can be applied in many cases to determine Cr valence at high-spatial resolution over a wide valence range.

2. Materials and methods

2.1. Chromium valence standards

The following high purity oxidation state standards were analyzed by EELS: conjectured low-spin [75] Cr^0, conjectured low-spin [75] $Cr^0_{23}C_6$, low-spin [75] $Cr^0(CO)_6$ {hexacarbonylchromium}, conjectured low-spin $(C_6H_6)_2Cr^{I}I$ {*bis*(benzene) chromium(I) iodide}, conjectured high-spin $Cr^{II}Se$, high-spin [20] $Cr^{II}F_2$, high-spin [20] $Cr^{II}Cl_2$, low-spin (see Ref. [76,77]) $[(CH_3)_5C_5]_2Cr^{II}$ {*bis*(pentamethylcyclopentadienyl)Cr also known as decamethylchromocene}, low-spin (see Ref. [77]) $[(CH_3)_4C_5H]_2Cr^{II}$ {*bis*(tetramethylcyclopentadienyl)Cr also known as octamethylchromocene}, low-spin [20] $Cr^{II}_2(CH_3COO)_4 \cdot 2H_2O$ {chromous acetate}, $Cr^{III}Cl_3$, $Cr^{III}_3(CH_3COO)_7(OH)_2$ {chromic acetate}, $LaCr^{III}O_3$, $Cr^{III}_2O_3$, $(Fe,Mg)(Cr^{III},Al,Fe)_2O_4$ {chromite}, $NdCr^{III}O_3$, $Cr^{III}PO_4 \cdot 4H_2O$, $KCr^{III}(SO_4)_2 \cdot 12H_2O$, $Cr^{IV}O_2$, $NdCr^{V}O_4$, $K_2Cr^{VI}O_4$, $PbCr^{VI}O_4$, $Na_2Cr^{VI}O_4$ and $K_2Cr^{VI}_2O_7$. The chromite was provided by Prof. T. Bernatowicz, and originated from the Tiebaghi Mine, New Calendonia. The $(C_6H_6)_2CrI$ compound was custom synthesized by Chemica Technologies (Bend, OR) and was shipped sealed under an atmosphere of argon. Electropolished Cr disks were provided by B. Kestel, and were shipped sealed under vacuum in a quartz tube. The Nd–Cr oxides were provided by Dr. H. Konno, and details of the structure and synthesis of $NdCrO_4$ have been previously described [78]. The chromous acetate was provided by Prof. P. Tregenna-Piggott and C. Dobe. The remainder of the standards was acquired from standard chemical supply sources.

All standards (with the exception of the electropolished Cr metal and $Cr(CO)_6$) were powdered, placed directly on Cu TEM grids coated with holey amorphous carbon, and analyzed immediately following preparation. All air-sensitive specimens were stored, powdered (if appropriate) and mounted in the TEM holder inside an oxygen-free (95% N_2:5% H_2) anaerobic chamber. For preparation of air-sensitive, hydrophilic specimens, desiccant beads were placed in the anaerobic chamber to reduce humidity below 18%. Each mounted specimen was kept under anaerobic conditions during transfer to the TEM column, and a nitrogen-purged glove bag affixed to the TEM goniometer facilitated insertion of the specimen holder under anaerobic conditions. The compound $Cr(CO)_6$ has a reported vapor pressure of 0.05 Torr at 36 °C (0.76 Torr at 74 °C) [79], therefore powdered $Cr(CO)_6$ was analyzed in the TEM column at a pressure of 70 Torr N_2 using an environmental cell (EC)-TEM holder.

Chromium compounds that exhibited strong electron-beam sensitivity (e.g., $K_3Cr^{V}O_8$) were not analyzed further. Compounds that exhibited mild electron-beam sensitivity were analyzed using low-electron fluences with a greatly desaturated filament, provided the compound exhibited no substantial systematic difference in Cr-$L_{2,3}$ spectra between grains exposed only briefly to electrons during EELS measurement and the same grains exposed to electrons for extended periods.

2.2. Transmission electron microscopy

A JEOL JEM-3010 analytical transmission electron microscope, operating at 300 keV with a LaB_6 filament,

and a measured point-to-point resolution of 2.1 Å was used for microcharacterization. This instrument is equipped with a side-entry motorized five axes goniometer, a Noran energy dispersive X-ray spectroscopy (EDXS) system, a Gatan 764 multiscan camera (MSC), a Gatan imaging filter (GIF200) capable of EELS and a JEOL EC system. The EC-TEM system used in this study has been previously described [72–74], and is of the closed cell design [80].

2.3. EELS experimental parameters and analysis

The following conditions were used during collection of EELS spectra under TEM and EC-TEM conditions: an illumination angle $2\alpha = 4-10$ mrad, a collection angle of $2\beta = 11.2 \pm 0.3$ mrad, a 2-mm-diameter entrance aperture and an energy dispersion of 0.1 eV/channel. Spectra were collected in diffraction mode of the transmission electron microscope (i.e. image coupling to the EELS spectrometer) and were corrected for dark current and channel-to-channel gain variation of the charge coupled device (CCD) detector.

The GIF spectrometer was calibrated to yield the energy, 855.00 ± 0.02 eV, for the edge maxima of Ni-L_3 (NiO). The reported calibration error is based on the standard error of the mean of 64 measurements. The Ni-L_3 edge of NiO is generally used to calibrate electron energy loss spectrometers because it has a small (0.2–0.25 eV) chemical shift [81,82]. However, there is uncertainty in the absolute energy position of the NiO Ni-L_3 edge, and consequently the value assigned to the NiO Ni-L_3 edge for EELS calibration varies in the literature by at least 3.5 eV. Further, the choice of using the edge onset or the position of the edge maxima for energy calibration also varies. Edge maxima are used for calibration here, because they are less affected by instrumental energy resolution and consequently are better defined than edge onsets. Since the most common value assigned to the Ni-L_3 edge of NiO in the literature appears to be 855 eV for the edge maximum, this integer value was used in this work. Although the actual value of the reference energy used for calibration is not crucial, it is critically important that the standard and experimental data are calibrated to the same energy reference and that this value is reported.

Four spectra were collected in rapid succession for each acquisition series: a zero-loss, O-K/Cr-L core-loss, a second zero-loss and a third zero-loss spectrum. Crucial for precise energy measurements, the Cr-L_3 edge maximum (with the drift tube set to the appropriate value) was within 20 spectrometer channels of the first zero-loss peak (with the drift tube set to zero); i.e. the null method was used. The criterion for selecting the position of the first zero-loss peak and the drift-tube offset was that the first spectrometer channel corresponded to ≈ 520 eV when the non-zero, drift-tube offset was applied. A second zero-loss peak was collected with the drift tube set to zero, and it was used to measure energy drift during core-loss measurement. A third zero-loss peak (offset to channel 100 of the spectrometer by applying the appropriate drift-tube offset) was collected for Fourier deconvolution of the core-loss spectra. Low-loss spectra were acquired with an integration time of 0.128 s (15 spectra were summed). Core-loss spectra covering the O-K/Cr-L regime were acquired with an integration time 2 s (15–90 spectra were summed). The energy scale of the core-loss spectra was calibrated using the mean position of the first two zero-loss peaks and the difference in energy of those zero-loss peaks represented the calibration error due to energy drift. The mean of the absolute values of the calibration errors arising from energy drift during spectra acquisition of the standards was 0.172 eV (i.e., ± 0.086 eV). In comparison, the energy resolution of the spectrometer was ~ 0.7 eV, measured as the full-width at half-maximum (FWHM) of the zero-loss peak.

By averaging results from a large number of measurements, accuracies greater than the instrument resolution can be obtained. Therefore for each standard, EELS spectra sets were collected from at least 30 individual grains. This also allowed the range of possible specimen heterogeneity in the standard to be sampled and this would be reflected in part by the scatter in the data. Pre-edge background subtraction and Fourier deconvolution of the spectra were performed using Gatan software. Parameterization of the Cr-$L_{2,3}$ fine structure was performed using stand-alone software, *Lanalysis*, written and compiled specifically for the analysis. For each standard, the results were averaged (data which deviated from the standard deviation of the mean by greater than a factor of 2.5 were excluded) and reported with the statistical standard error.

All standards were analyzed within a 27 day continuous time frame over which time the spectrometer electronics and TEM high voltage were continuously energized. The first standard analyzed was reanalyzed after all other standards had been examined. The difference in mean L_3 peak position for the duplicate runs of the first standard was 0.28 eV. Therefore, differences in energy calibration between any two standards due to drift of the GIF200 spectrometer over 27 days is no greater than 0.28 eV, assuming linear drift.

3. Results and discussion

A comparison of the EELS core-loss spectra over an energy range 520 to 600 eV (including the O-K and Cr-$L_{2,3}$ edges) from Cr standards of known valence is shown in Fig. 1. Differences in O-K edge fine structure presumably reflect the diversity in O bonding among the compounds, although O-K fine structure is not analyzed in this work. However, the lack of a significant O-K edge in EELS spectra of Cr metal and $Cr_{23}C_6$ is used to affirm that these specimens had minimal surface oxidation and are reliable zero-valence standards.

Systematic differences in Cr-$L_{2,3}$ fine structure are apparent in the spectra of the oxidation state standards. For example, the Cr-$L_{2,3}$ edges for the standards show a

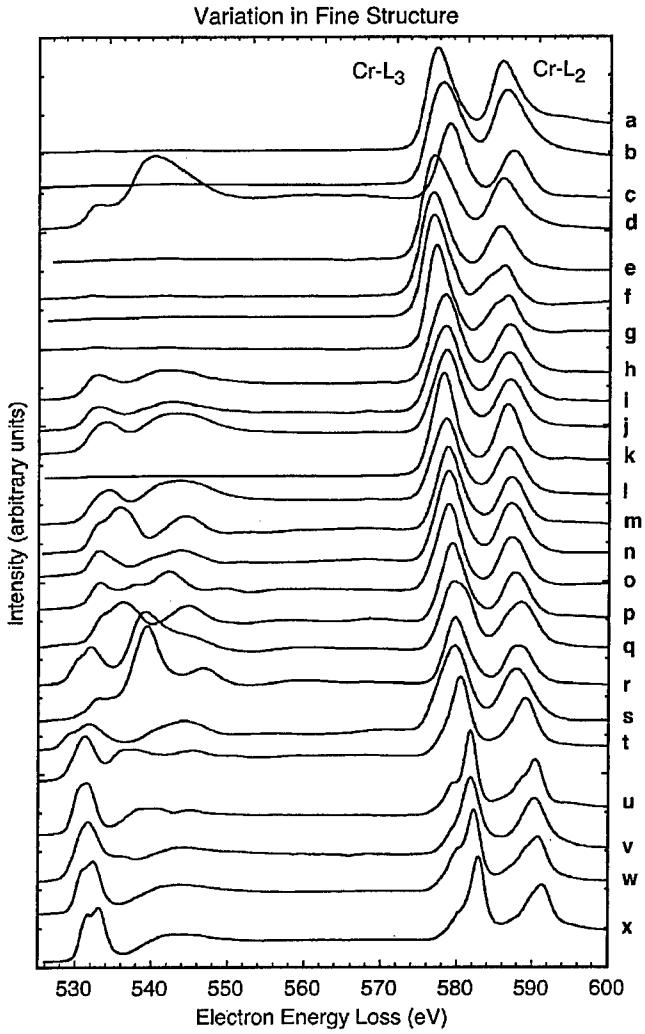

Fig. 1. Electron energy loss spectra of (a) conjectured low-spin [75] Cr^0, (b) conjectured low-spin [75] $Cr^0_{23}C_6$, (c) low-spin [75] $Cr^0(CO)_6$, (d) conjectured low-spin $(C_6H_6)_2Cr^{I}I$ {*bis*(benzene) chromium(I) iodide}, (e) conjectured high-spin $Cr^{II}Se$, (f) high-spin [20] $Cr^{II}F_2$, (g) high-spin [20] $Cr^{II}Cl_2$, (h) low-spin [76,77] $[(CH_3)_5C_5]_2Cr^{II}$ {*bis*(pentamethylcyclopentadienyl)chromium also known as decamethylchromocene}, (i) low-spin [77] $[(CH_3)_4C_5H]_2Cr^{II}$ {*bis*(tetramethylcyclopentadienyl)-chromium also known as octamethylchromocene}, (j) low-spin [20] $Cr^{II}_2(CH_3COO)_4 \cdot 2H_2O$ {chromous acetate}, (k) $Cr^{III}Cl_3$, (l) $Cr^{III}_3(CH_3COO)_7(OH)_2$ {chromic acetate}, (m) $LaCr^{III}O_3$, (n) $Cr^{III}_2O_3$, (o) $(Fe,Mg)(Cr^{III},Al,Fe)_2O_4$ {chromite}, (p) $NdCr^{III}O_3$, (q) $Cr^{III}PO_4 \cdot 4H_2O$, (r) $KCr^{III}(SO_4)_2 \cdot 12H_2O$, (s) $Cr^{IV}O_2$, (t) $NdCr^{V}O_4$, (u) $K_2Cr^{VI}O_4$, (v) $PbCr^{VI}O_4$, (w) $Na_2Cr^{VI}O_4$, and (x) $K_2Cr^{VI}_2O_7$. For Cr(0)–Cr(II), d^n orbital spin configuration is specified when found reported in literature. Spectra were offset from one another vertically and were normalized so that the intensity of the L_3 peaks was equal. Spectra shown for the Cr standards represent the sum of upwards of thirty individual spectra.

systematic shift in peak position to higher energy with increasing valence from Cr(I) to Cr(VI). The peak height of the L_3 edge relative to the L_2 edge generally decreased with increasing oxidation state from Cr(II) to Cr(VI). In addition, the Cr-$L_{2,3}$ edges of Cr(VI) are further differentiated in that they appear asymmetric because each is split into two not fully resolved peaks separated by ~2 eV.

3.1. Parameterization of Cr-$L_{2,3}$ fine structure

The fine structure of the Cr-$L_{2,3}$ edge was parameterized by measurement of the chemical shift of the L_3 edge and the L_3/L_2 ratio of integrated-peak intensity under the $L_{2,3}$ edges. The positions of the L_3 edge [60] and the L_3/L_2 ratio [60,62] for many transition metals have been shown by previous EELS work to be dependent on valence. Nearly all EELS studies to determine metal valence have been based on the analysis of only one parameterization of the fine structure, although different parameterizations have been utilized. In our earlier studies [72–74], two common parameterizations were used in combination to provide higher confidence and accuracy in the valence determination. However, an important result of our present work is that we show that neither parameterization alone can be used to unambiguously determine Cr oxidation state if the full range of possible valences is considered.

3.2. EELS L_3 peak positions and comparison to XPS binding energies

For the measurement of chemical shift, L_3 edges are more suitable than L_2 edges because their intrinsic line widths are narrower and peak maxima are better defined. The extra broadening of the L_2 threshold peak results from the shorter lifetime of the excited state associated with L_2 which can decay by an extra Coster–Kronig Auger decay channel not available for the excited state associated with the L_3 edge (e.g., see Ref. [83]). The EELS L_3 absorption edge maxima were determined from the channel with maximum counts, and the results for Cr oxidation state standards are summarized in Table 1 together with EELS Cr-L_3 edge maxima reported in the literature.

Unfortunately, the energy calibration of EELS spectrometers (usually based on the NiO Ni-L_3 edge) often vary in the literature or are not explicitly stated. For proper comparison with our measurements, where possible, the literature values in Table 1 were recalibrated to the NiO Ni-L_3 edge maxima at 855 eV (calibration used in this work). Among the recalibrated values from the literature and our measurements (Table 1), L_3 peak positions vary by $< \pm 2.2$ eV for any one Cr compound measured by different researchers.

For comparison to EELS measured Cr-L_3 edge maxima, literature values of XPS measured core-level (or inner-shell) binding energies of Cr compounds are shown in Table 2. In XPS, a bulk specimen is illuminated with monochromatic X-rays and the kinetic energies of ejected photoelectrons are measured. The EELS edge onset, the sudden rise in intensity preceding each of the $L_{2,3}$ peaks, represents the ionization threshold, which *approximately* corresponds to the inner-shell binding energy measured by XPS. Various methods are used for referencing XPS-measured binding energies that lead to differences of up to 0.5 eV in reported energies [84]. The literature values in Table 2 are recalibrated to a Au $4f_{7/2}$ line at 84.0 eV. The

Table 1
Cr-L_3 ($2p_{3/2}$) and Cr-L_2 ($2p_{1/2}$) adsorption-edges: EELS—edge maxima[a]

Compound	Formal valence	Cr-L_3 ($2p_{3/2}$) (eV)	Cr-L_2 ($2p_{1/2}$) (eV)	Reference
$Cr_{20}Au_{80}$ [cLS]	0	570.6	580.2	Pease et al. (1986)[b] [88]
Cr [cLS]	0	573.6	582.1	Pease et al. (1986)[b] [88]
		575.5±1.1	584.0±1.1	Leapman et al. (1982)[c,d,g] [81]
		577.18±0.02	585.79±0.02	This study
$Cr_{23}C_6$ [cLS]	0	578.03±0.05	586.40±0.03	This study
$Cr(CO)_6$ [LS]	0	579.06±0.07	587.34±0.08	This study
$(C_6H_6)_2CrI$ [cLS]	I	576.87±0.03	585.97±0.04	This study
CrSe [cHS]	II	576.65±0.05	585.60±0.04	This study
CrF_2 [HS]	II	576.78±0.03	586.15±0.03	This study
$CrCl_2$ [HS]	II	577.11±0.04	586.66±0.04	This study
$[(CH_3)_5C_5]_2Cr$ [LS]	II	578.35±0.02	586.83±0.03	This study
$[(CH_3)_4C_5H]_2Cr$ [LS]	II	578.43±0.04	586.77±0.03	This study
$Cr_2(CH_3COO)_4 \cdot 2H_2O$ [LS]	II	578.55±0.03	586.95±0.03	This study
Cr_2O_3	III	577.1±1.1	584.7±1.1	Leapman et al. (1982)[c,d,g] [81]
		578.3	586.4	Krivanek and Paterson (1990)[e,g] [89]
		578.81±0.03	587.17±0.03	This study
		580.6±0.3	588.7±0.3	Suzuki and Tomita (1997)[b] [90]
$CrCl_3$	III	578.13±0.02	586.61±0.02	This study
$Cr_3(CH_3COO)_7(OH)_2$	III	578.47±0.02	586.81±0.02	This study
$LaCrO_3$	III	578.71±0.02	587.16±0.03	This study
$(Fe,Mg)(Cr,Al,Fe)_2O_4$	III	578.89±0.02	587.24±0.02	This study
		579.8±0.2	587.8±0.2	Garvie et al. (1994)[f,g] [91]
$NdCrO_3$	III	579.35±0.03	587.68±0.03	This study
$Ca_{1.1}(Cr,Fe,Mg)_4(SiAl)_8$-, $(Si,Al)_8O_{20}(OH)_4 \cdot nH_2O$	III	579.7±0.2	587.9±0.2	Garvie et al. (1994)[f,g] [91]
$CrPO_4 \cdot 4H_2O$	III	579.74±0.06	588.57±0.05	This study
$KCr(SO_4)_2 \cdot 12H_2O$	III	579.77±0.04	588.18±0.08	This study
CrO_2	IV	579.70±0.03	587.83±0.03	This study
		581.8±0.3	589.6±0.3	Suzuki and Tomita (1997)[b] [90]
$NdCrO_4$	V	580.43±0.03	589.05±0.03	This study
K_2CrO_4	VI	581.77±0.02	590.41±0.02	This study
$PbCrO_4$	VI	581.85±0.07	590.34±0.06	This study
		582.1±0.2	590.7±0.2	Garvie et al. (1994)[f,g] [91]
Na_2CrO_4	VI	582.26±0.03	590.77±0.03	This study
$K_2Cr_2O_7$	VI	582.83±0.03	591.35±0.03	This study
		583.6±0.3	592.3±0.3	Suzuki and Tomita (1997)[b] [90]

cLS—conjectured low spin Cr d^n configuration.
LS—low spin Cr d^n configuration.
cHS—conjectured high spin Cr d^n configuration.
HS—high spin Cr d^n configuration.
[a]EELS L-edge peak positions are calibrated to NiO Ni-L_3 maxima at 855.0 eV.
[b]Energy calibration not reported. Although the L-edge maxima cannot be directly compared to our study, the relative energy differences in L-edge maxima between specimens from the same study can be compared to our study.
[c]EELS L-edge onsets reported in reference, however L-edge maxima are shown here.
[d]After recalibrating the EELS NiO Ni-L_3 edge maximum to 855.0 from 856.3 eV (determined to have been used in reference).
[e]After recalibrating the EELS NiO Ni-L_3 edge maximum to 855.0 from 852.75 eV used in reference.
[f]After recalibrating the EELS NiO Ni-L_3 edge maximum to 855.0 from 853.2 eV used in reference.
[g]Recalibrated peak position = old peak position × (old Ni-L_3 edge maximum)/855.0 eV.

recalibrated binding energies for any given Cr compound measured by the different XPS studies (Table 2) vary by $< \pm 0.7$ eV. The factor of three smaller variation in literature reported Cr-L_3 XPS binding energies compared to the variation in literature reported EELS edge maxima can partially be explained by the higher energy resolution of XPS over EELS.

A comparison of the EELS Cr-L_3 peak positions measured in this work and the mean XPS binding energies from Table 2, for compounds measured by both techniques, is shown in Fig. 2. Only a qualitative comparison can be made because of instrumental differences in the collection of the data. Nevertheless, the slope of the linear least-squares fit in Fig. 2 suggests XPS measured binding

Table 2
Cr-L_3 ($2p_{3/2}$) and Cr-L_2 ($2p_{1/2}$) adsorption-edges: XPS-binding energies[a]

Compound	Formal valence	Cr-L_3 ($2p_{3/2}$) (eV)	Cr-L_2 ($2p_{1/2}$) (eV)	Reference
Cr [cLS]	0	573.8	583.0	Allen et al. (1976) [92]
		574.07	583.43	Asami and Hashimoto (1977)[b,c,d] [93]
		574.1		Moffat et al. (1995) [94]
CrP [cLS]	0	574.2		Moffat et al. (1995) [94]
$Cr(CO)_6$ [LS]	0	577.6	586.3	Allen et al. (1976) [92]
		578.5	587.5	Clark and Adams (1971) [95]
$LaCrO_3$	III	576.1±0.09	585.8±0.05	Konno et al. (1992) [96]
$CrPO_4 \cdot 4H_2O$	III	576.4±0.2		Neal et al. (2002) [46]
$CuCrO_2$	III	576.4±0.2	586.2±0.2	Allen et al. (1973)[c,d] (1976) [51,92]
Cr_2O_3	III	576.45	585.96	Asami and Hashimoto (1977)[b,d] [93]
		576.6–576.8		Moffat et al. (1995) [94]
		576.8±0.2	586.5±0.2	Allen et al. (1973)[c,d] (1976) [51,92]
		576.8	586.7	Ikemoto et al. (1976) [97]
$Cr_3(OH)_2(OOCCH_3)_7$	III	576.5±0.2		Neal et al. (2002) [46]
$Cr(OH)_3 \cdot nH_2O$	III	576.96	586.31	Asami and Hashimoto (1977)[b,d] [93]
		577.1		Moffat et al. (1995) [94]
$NaCrO_2$	III	577.0±0.2	586.9±0.2	Allen et al. (1973)[c,d] (1976) [51,92]
CrOOH	III	577.0	586.9	Ikemoto et al. (1976) [97]
$LiCrO_2$	III	577.0±0.2	586.8±0.2	Allen et al. (1973)[c,d] (1976) [51,92]
CrP	III	577.4		Moffat et al. (1995) [94]
$CrCl_3 \cdot 6H_2O$	III	577.5		Moffat et al. (1995) [94]
$Cr(CH_3COCHCOCH_3)_3$	III	577.7	587.4	Allen et al. (1976) [92]
$CrCl_3$	III	577.8	587.4	Allen et al. (1976) [92]
$CrPO_4$	III	577.8		Moffat et al. (1995) [94]
$CrBO_3$	III	578.0		Moffat et al. (1995) [94]
$Cr(C_2H_8N_2)_3Cl_3$	III	578.3	588.0	Allen et al. (1976) [92]
$Cr(NH_3)_6Cl_3$	III	578.5	588.2	Allen et al. (1976) [92]
$Cr_2(SO_4) \cdot 15H_2O$	III	578.6		Moffat et al. (1995) [94]
$(NH_4)_3CrF_6$	III	579.5	589.7	Allen et al. (1976) [92]
$Cr_2(CO_4)_3 \cdot nH_2O$	III	580.2	589.8	Allen et al. (1976) [92]
$Cr(CF_3COCHCOCF_3)_3$	III	580.6	589.6	Clark and Adams (1971) [95]
$KCr(SO_4)_2 \cdot 12H_2O$	III	581.0	590.5	Allen et al. (1976) [92]
K_3CrF_6	III	583.0	593.2	Allen et al. (1976) [92]
CrO_2	IV	576.3	586.0	Ikemoto et al. (1976) [97]
$LaCrO_4$	V	578.8±0.21	588.0±0.22	Konno et al. (1992) [96]
CrO_3	VI	578.3±0.2	587.0±0.02	Allen et al. (1973)[c,d] [51]
		579.00	588.26	Asami and Hashimoto (1977)[b,d] [93]
$CaCrO_4$	VI	578.9±0.2	588.1±0.2	Allen et al. (1973)[c,d] (1976) [51,92]
$BaCrO_4$	VI	579.1±0.2	588.4±0.2	Allen et al. (1973)[c,d] (1976) [51,92]
$K_2Cr_2O_7$	VI	579.4±0.2	588.8±0.2	Allen et al. (1973)[c,d] (1976) [51,92]
		579.8	589.1	Ikemoto et al. (1976) [97]
$Na_2Cr_2O_7$	VI	579.4±0.2	588.5±0.2	Allen et al. (1973)[c,d] (1976) [51,92]
$Rb_2Cr_2O_7$	VI	579.4±0.2	588.7±0.2	Allen et al. (1973)[c,d] (1976) [51,92]
$Cs_2Cr_2O_7$	VI	579.5±0.2	588.7±0.2	Allen et al. (1973)[c,d] (1976) [51,92]
$SrCrO_4$	VI	579.6±0.2	588.6±0.2	Allen et al. (1973)[c,d] (1976) [51,92]
K_2CrO_4	VI	579.6±0.2	588.9±0.2	Allen et al. (1973)[c,d] (1976) [51,92]
Cs_2CrO_4	VI	579.8±0.2	588.8±0.2	Allen et al. (1973)[c,d] (1976) [51,92]
Li_2CrO_4	VI	579.8±0.2	589.0±0.2	Allen et al. (1973)[c,d] (1976) [51,92]
Na_2CrO_4	VI	579.8±0.2	589.1±0.2	Allen et al. (1973)[d] (1976) [51,92]

cLS—conjectured low spin Cr d^n configuration.
LS—low spin Cr d^n configuration.
[a]XPS binding energies are calibrated to Au $4f_{7/2}$ line at 84.0 eV.
[b]After recalibrating the XPS Au $4f_{7/2}$ line to 84.0 from 84.07 eV used in reference.
[c]After recalibrating the XPS Au $4f_{7/2}$ line to 84.0 from 82.8 eV used in reference.
[d]Recalibrated peak position = old peak position + (84.0 eV − old Au $4f_{7/2}$ line), see Refs. [51,92].

energies of Cr are on average 0.36% less than EELS measured edge maxima. Egerton (1996) [85] has suggested differences in chemical shift measured by XPS and EELS may arise from many-body relaxation effects (more dominant in XPS) in which nearby electron orbitals are pulled towards a core hole. Further, it has been suggested

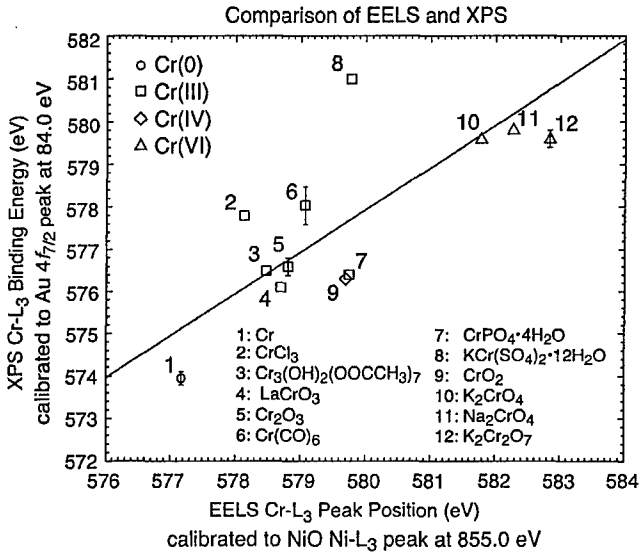

Fig. 2. Comparison of the EELS measured Cr-L_3 edge maxima (from this study, see Table 1) with XPS measured binding energies from Table 2. Vertical error bars correspond to the range in XPS binding energies cited in Table 2. The line corresponds to a linear least-squares fit, $y = mx$, that yielded $m = 0.9964$ with fit factor of $R = 0.72555$.

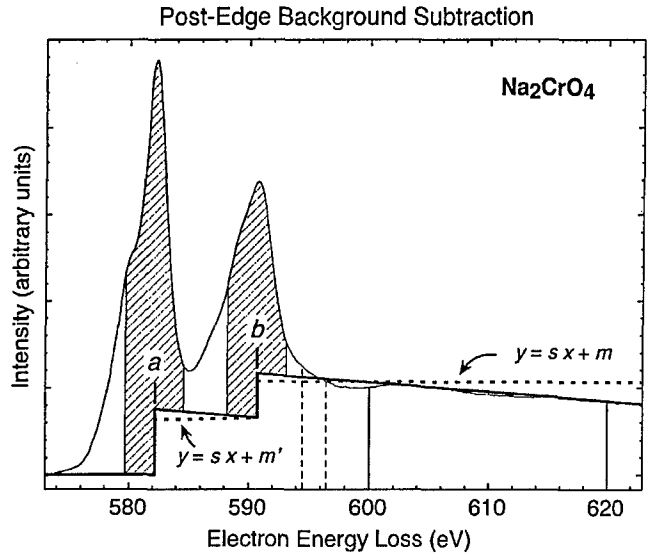

Fig. 3. Background subtraction used in method I (bold line) and method II (dashed bold line) to remove background under the L_2 edge, arising from the tail contributions of the L_3 edge. The fitting parameters a, b, s and m are: the L_3 maximum; the L_2 maximum; the slope and intercept of the linear function fitted to the post-edge region. The parameter m' is given by $m' = (bm-as)/(1+\rho)$, where ρ represents the branching ratio (i.e., L_3/L_2 ratio). For method I, the post-edge background was fit to a window between 600–620 eV (solid vertical lines). For method II, $s \equiv 0$ and the post-edge background was fit to a 2-eV-wide window that started 4.8 eV above the L_2 edge maximum (dashed vertical lines). The intensity under the L-edges was measured by integrating 5-eV-wide regions (cross-hatched areas), centered with respect to the L-edge maxima.

that the presence of core holes increase the effective attraction between a nucleus and electrons resulting in deeper electronic shell energies shifting the apparent binding energy [82]. Since electrons are ejected with higher energies with XPS than in EELS, this effect is thought to be stronger for XPS [82]. Further, the absolute difference between XPS binding energies and EELS edge maxima could vary somewhat with the electronic structure (i.e., the compound). With these points in mind, the trend in the XPS measured chemical shifts is largely consistent with our EELS measurements.

3.3. *EELS L_3/L_2 ratio of integrated intensity*

Measurement of the L_3/L_2 ratio of integrated peak intensity is *very* sensitive to analysis conditions such as peak integration widths and background subtraction methods that remove intensity due to transitions to unoccupied states in the continuum. Therefore, a detailed description of the procedure to quantify the L_3/L_2 ratio is given and it is as follows. The Cr-L_3 pre-absorption edge background was fit to a power law and subtracted. Plural inelastic scattering was removed by Fourier deconvolution methods [85] and the mean counts in a 5 eV window preceding the onset of the Cr-L_3 edge was normalized to zero. The background intensity under the L_2 edge, arising from the tail contributions of the L_3 edge, was then subtracted using either of two methods. The first method is similar to the two-step function used by Pearson et al. [86], and is illustrated in Fig. 3. A two-step function was defined by fitting a linear function to the Cr-L_2 post-edge region over a 20 eV window (extending from 600 to 620 eV). This function was extrapolated to the L_2 maximum where a linear step was inserted and a linear function (of the same slope as that fitted to the Cr-L_2 post-edge region) was extrapolated into the L_3 threshold. A second step was inserted at the L_3 maximum and set to zero below the L_3 maximum. The ratio for the step heights should scale with the L_3/L_2 ratio, the unknown parameter to be measured following background subtraction. As a first-order approximation, the ratio for the step heights was initially set at 2:1, consistent with the multiplicity of the initial states, that of four $2p_{3/2}$ electrons and two $2p_{1/2}$ electrons. The step height ratio was refined through iteration. The step height ratio of iteration $n+1$ was assigned the mean L_3/L_2 ratio determined by iteration n. The L_3/L_2 ratio was determined by integrating the two edges over a 5 eV window centered with respect to each edge maximum (Fig. 3).

Although the first subtraction method approximates the decreasing background, often Cr-L_2 post-edge features remained following Fourier deconvolution. Variation in residual post-edge features between spectra introduced scatter in the resultant L_3/L_2 ratios. To reduce scatter, a second method using a zero-slope, two-step function was applied. The second background fitting procedure is identical to the first except the slope of the linear function is set to zero and fit to a 2 eV window positioned above the L_2 edge maximum prior to the post-edge features. The

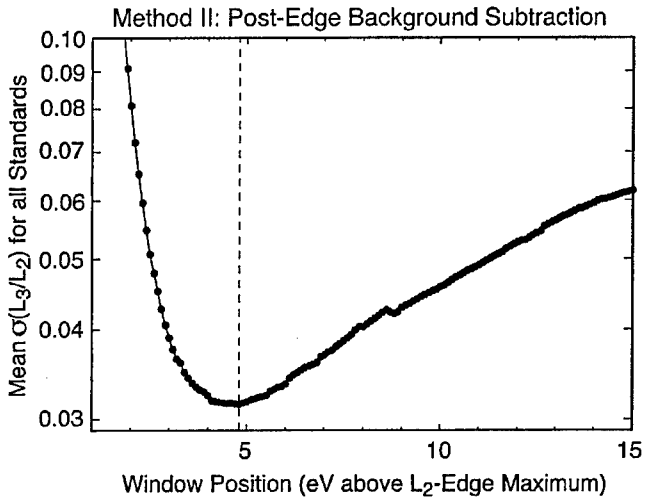

Fig. 4. Scatter in measured L_3/L_2 ratios as a function of position of the method II background window (2 eV width). Scatter is represented by the average of all σ_i, where i denotes the Cr compound and σ is the standard deviation of the mean L_3/L_2 ratio. The minimum in the scatter of the L_3/L_2 ratios occurs at a window position starting at 4.8 eV above the Cr-L_2 edge maximum.

L_3/L_2 ratios and the scatter in their values depend on the position of the post-edge fitting window. The window position selected, 4.8 eV above the Cr-L_2 edge maximum, was the one that yielded minimum total scatter for the set of 24 Cr standards (see Fig. 4). The window position was defined with respect to the mean energy of the Cr-L_2 edge maximum for a given standard, because the mean energy was a more accurate measurement of the edge maximum than that determined from any individual spectrum.

The L_3/L_2 peak ratios for the Cr standards are summarized in Table 3 for $n = 1$ and 10 iterations of the step height ratio. The mean differences between L_3/L_2 ratios determined with $n = 1$ and 10 iterations are $\approx 0.4\%$ (method I) and 0.5% (method II). Therefore, an approximation of 2:1 for the step height ratio yields accurate results. Nevertheless, iteration yielded less scatter in the data, a reduction of 2.8% (method I) and 4.1% (method II) in the mean standard error of the L_3/L_2 ratios for the Cr compounds (Fig. 5). Furthermore, it is straightforward to write the analysis software to iterate the calculations, and the L_3/L_2 ratio converged quickly with $\Delta(L_3/L_2) < \pm 10^{-5}$ after five iterations. Therefore, it requires little extra effort to determine the step height ratio by iteration. In direct comparison of the two background subtraction methods, method II yielded mean standard errors for the L_3/L_2 ratios that were roughly half that yielded by method I. This is illustrated in Fig. 5 which plots the standard deviation of the measured L_3/L_2 ratios for each standard determined by the two background subtraction methods for $n = 1$ and 10 iterations of the step height ratio. Method II with $n = 10$ iterations yields the lowest standard deviations for the measured L_3/L_2 ratios, and therefore, results from method II ($n = 10$) are used in the following sections.

3.4. Correlation of $L_{2,3}$ fine-structure parameterizations to valence

The correlation between the parameterizations of the $L_{2,3}$ edge fine structure to Cr valence of the standards is shown in Fig. 6. Data for individual Cr standards are fairly well clustered with the scatter reflecting specimen heterogeneities and instrumental instabilities. The high-spin compounds may have an additional factor contributing to their scatter because they exhibit the greatest scatter in L_3/L_2 ratio (a factor of $\approx 3\times$ that of the other standards). The mean spread in the data for a Cr compound is ± 0.36 eV for the L_3 position and ± 0.057 for the L_3/L_2 ratio, corresponding to $\approx \pm 5\%$ the total range of the correlation plot along both axes.

It is important to recognize that the electron configuration of an atom is responsible for the fine structure of its absorption edges and other factors in addition to valence can influence $L_{2,3}$ fine structure, such as crystal field splitting (e.g. atom coordination, low- or high-spin d^n configuration), spin–orbit interactions, atomic coulomb repulsion and exchange effects. Because of these effects, different compounds of the same Cr valence disperse within bounded regions in the correlation plot (Fig. 6). As shown in Fig. 6, the d^n orbital configuration has a large effect on $L_{2,3}$ fine structure, and transition metals with 4–7 electrons in the d^n orbital can exist in either a low- or high-spin state, such as Cr(0) to Cr(II). The low-spin and high-spin compounds of Cr(II), respectively, cluster in two separated regions in the correlation plot. The observed lower L_3 peak energy and larger L_3/L_2 ratio for low-spin as compared to high-spin Cr(II) are comparable in magnitude and direction to those observed between low-spin and high-spin Fe(II) in Fe^{II}(1,10-phenanthroline)$_2$(NCS)$_2$ which exhibits a $3d^6$ orbital spin-transition at $T_c = 176$ K (see Ref. [87]). Since organometallic Cr compounds are usually of low-spin state, the organometallic Cr(I) compound analyzed in this work is likely also low spin. If correct, and if high-spin Cr(I) behaves similarly to high-spin Cr(II) and high-spin Fe(II) in Fe^{II}(1,10-phenanthroline)$_2$(NCS)$_2$ with regard to their low-spin counterparts, then high-spin Cr(I) should lie to the left of the high-spin Cr(II) region. Further, it has been reported that all known Cr(0) compounds are of low-spin state [75].

3.5. Chromium valence determination

It is difficult to explicitly deconvolve the influences of valence from the other factors affecting fine structure. The fine-structure correlation plot represents a map of the range in fine structure (including influences from factors other than valence) that a Cr atom of a particular valence can display. Since many of the valence/spin-state regions are well separated, the correlation plot can be used to determine the mean Cr valence (or at least constrain the possible valence range) of an unknown by plotting the L_3 peak energy and L_3/L_2 ratio of the unknown. It is

Table 3
Cr-L adsorption edge ratios

Compound	L_3/L_2 integrated ratio			
	Background method 1 Pearson et al. (1993) [86]		Background method 2 Zero-slope two step	
	$n=1$	$n=10$	$n=1$	$n=10$
$Cr^0_{23}C_6$ cLS	1.324±0.007	1.315±0.007	1.511±0.003	1.498±0.003
$Cr^0(CO)_6$ LS	1.419±0.020	1.416±0.019	1.525±0.007	1.520±0.007
Cr^0 cLS	1.389±0.003	1.377±0.003	1.540±0.003	1.525±0.003
$(C_6H_6)_2Cr^II$ cLS	1.631±0.011	1.620±0.010	1.807±0.007	1.798±0.006
$[(CH_3)_4C_5H]_2Cr^{II}$ LS	1.612±0.012	1.605±0.012	1.723±0.004	1.715±0.004
$Cr^{II}_2(CH_3COO)_4\cdot 2(H_2O)$ LS	1.633±0.007	1.630±0.006	1.729±0.003	1.720±0.002
$[(CH_3)_5C_5]_2Cr^{II}$ LS	1.620±0.017	1.616±0.016	1.762±0.004	1.757±0.003
$Cr^{II}Se$ cHS	1.899±0.022	1.895±0.022	2.004±0.013	2.004±0.013
$Cr^{II}Cl_2$ HS	2.311±0.044	2.327±0.045	2.178±0.017	2.184±0.017
$Cr^{II}F_2$ HS	2.386±0.025	2.400±0.026	2.240±0.014	2.246±0.014
$Cr^{III}PO_4\cdot 4H_2O$	1.490±0.004	1.489±0.005	1.554±0.003	1.546±0.003
$KCr^{III}(SO_4)_2\cdot 12H_2O$	1.508±0.009	1.504±0.009	1.565±0.005	1.559±0.005
$Cr^{III}Cl_3$	1.589±0.008	1.585±0.008	1.644±0.003	1.638±0.003
$(Fe,Mg)(Cr^{III},Al,Fe)_2O_4$	1.644±0.005	1.638±0.004	1.653±0.002	1.646±0.002
$NdCr^{III}O_3$	1.619±0.011	1.616±0.009	1.684±0.007	1.675±0.007
$LaCr^{III}O_3$	1.604±0.005	1.600±0.005	1.711±0.004	1.704±0.004
$Cr^{III}_3(CH_3COO)_7(OH)_2$	1.624±0.007	1.618±0.006	1.715±0.002	1.709±0.002
$Cr^{III}_2O_3$	1.679±0.013	1.671±0.012	1.720±0.006	1.712±0.005
$Cr^{IV}O_2$	1.484±0.002	1.478±0.002	1.556±0.002	1.548±0.002
$NdCr^{V}O_4$	1.398±0.006	1.387±0.005	1.426±0.005	1.414±0.004
$PbCr^{VI}O_4$	1.368±0.006	1.355±0.006	1.381±0.005	1.370±0.005
$K_2Cr^{VI}_2O_7$	1.397±0.006	1.387±0.006	1.418±0.006	1.408±0.006
$K_2Cr^{VI}O_4$	1.416±0.005	1.405±0.005	1.484±0.004	1.474±0.004
$Na_2Cr^{VI}O_4$	1.498±0.008	1.484±0.008	1.486±0.006	1.475±0.006

cLS—conjectured low spin Cr d^n configuration.
LS—low spin Cr d^n configuration.
cHS—conjectured high spin Cr d^n configuration.
HS—high spin Cr d^n configuration.

important that the correlation plot contain the broadest collection of standards, with as varied chemistry as feasible, to map the full range in fine structure of a particular valence. The better these ranges are known, the more confidence can be placed in any valence determination. In this regard, the data in Fig. 6 are supplemented by Table 2.

With only two fine-structure parameterizations, Cr valence determination is limited in that there are two areas in the correlation plot where the valence regions overlap, i.e. partial overlap of low-spin Cr(II) with the Cr(III) region and overlap of Cr(IV) with part of the Cr(0) and Cr(III) regions. Within these overlap areas additional data are required for unambiguous valence determination. For instance, further fine-structure parameterizations might be possible, however those that we evaluated provided no additional information on valence. The separation between the L_3 and L_2 edge maxima was nearly constant for the set of standards examined (see Table 2). Our attempts to quantify the total integrated $L_{2,3}$ (white-line) intensity normalized to background intensity resulted in large scatter in the measurement precluding correlation with valence. Although the measured FWHM of the L_3 edge tended to decrease with increasing valence, the range in the L_3 width exhibited for compounds of the same valence was rather large.

In nearly all previous EELS studies, only one fine-structure parameterization has been used to determine metal valence or quantify the ratio of two mixed valence states. However for Cr, the prospects of valence determination are severely limited if only one fine-structure parameterization is examined. Considering our two fine-structure parameterizations separately, there is significant overlap in the mean L_3/L_2 ratios between Cr(I), low-spin Cr(II) and Cr(III) as well as significant overlap between Cr(VI) and both Cr(V) and Cr(0). Even the stable species Cr(III) and Cr(VI) show slight overlap in mean L_3/L_2 ratios. Additionally, there is significant overlap in the mean L_3 peak energies between Cr(0), Cr(I) and Cr(II) as well as between Cr(0) and Cr(III). The overlap in mean L_3/L_2 ratios and mean L_3 peak energies for compounds of different Cr-valence underscores the influence of factors other than valence on fine structure. Consequently, it is not possible to unambiguously determine valence using either of the two fine-structure parameterizations alone unless only the stable species, Cr(III) and Cr(VI), are known to be

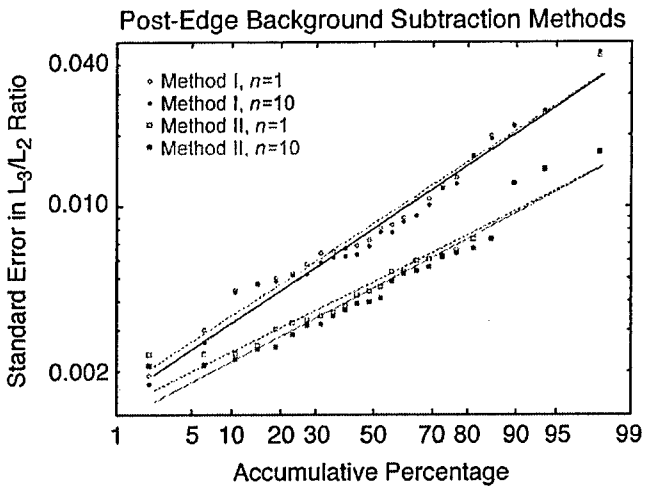

Fig. 5. Scatter in measured L_3/L_2 ratios as a function of background subtraction method and the number, n, of iterations used to determine the step height: method I, $n = 1$ (red open circle); method I, $n = 10$ (blue solid circle); method II, $n = 1$ (green open square) and method II, $n = 10$ (purple solid square). The standard error of the mean L_3/L_2 ratio measured for each Cr standard (Table 3) is plotted as accumulative percentages. Straight lines are linear least-squares fits to log normal distributions and serve as visual aids. The lower a set of data plots the less scatter is present in the L_3/L_2 measurements, and method II using $n = 10$ is shown to be the best analysis method that was examined.

present in the experimental sample. For the study of Cr redox intermediates, we demonstrate it is necessary to use multiple fine-structure parameterizations in combination. This will likely also be the case for other metals, such as Mn, that exhibit a wide valence range and low/high spin states for many valences.

4. Conclusions

We have correlated the fine structure of $L_{2,3}$ adsorption edges to Cr valence over the range Cr(0)–Cr(VI) using a large suite of specimens under identical instrumental conditions. Our results represent the most complete and systematic EELS study of the dependence of Cr-$L_{2,3}$ fine structure on Cr oxidation state. Our results illustrate well that other factors in addition to valence, e.g. crystal field splitting (i.e, atom coordination, low- or high-spin configuration), spin–orbit interactions, atomic coulomb repulsion and exchange effects, can significantly influence the fine structure of Cr-$L_{2,3}$ adsorption edges. In particular, we demonstrate that spin state of the d orbital has a significant influence on the fine structure of Cr-$L_{2,3}$ adsorption edges and must be taken into consideration in the determination of Cr valence. We further demonstrate that multiple parameterizations of the Cr-$L_{2,3}$ fine structure *must* be used together if valence is to be unambiguously determined when the full range of oxidation states is considered. This will likely also be the case for other metals, such as Mn, that exhibit a wide valence range and low/high spin states for many valences. In contrast, nearly all previous EELS techniques have utilized the measurement of only one fine-

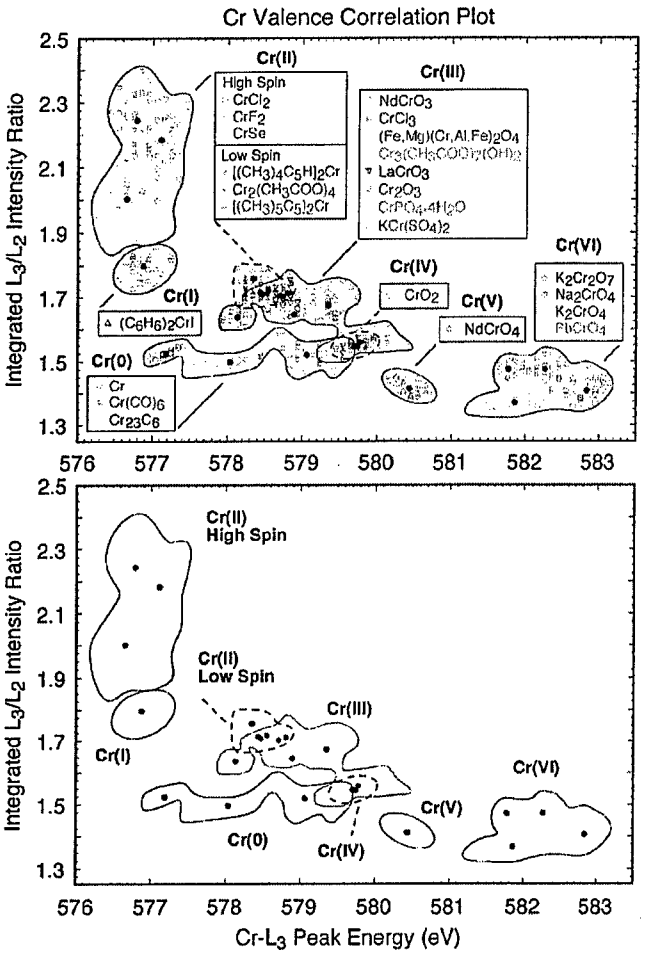

Fig. 6. Correlation between measured L_3/L_2 ratios and L_3 peak positions with respect to Cr valence for a set of valence standards. The L_3/L_2 ratios were determined using background subtraction method II with $n = 10$ iterations for determination of the step height ratio. Regions bounded by closed curves are visual guides. The different Cr oxidation states fall within largely separate regions and are labeled Cr(0), Cr(I), Cr(II), Cr(III), Cr(IV) and Cr(VI). The black, solid circles represent the mean of the data for a particular Cr standard. The Cr(0) and Cr(I) compounds are likely all of low-spin state. The spin state of the Cr(II) compounds is specified.

structure parameterization to determine metal valence. Although there are limitations in using two parameterizations for the valence determination of Cr, the correlation technique can be used to constrain the range of possible valences and in many cases determine Cr valence.

Acknowledgements

We thank Prof. T.J. Bernatowicz (Washington University, St. Louis, USA) for kindly providing natural chromite, Bernard Kestel (Argonne National Laboratory, USA) for kindly providing electropolished Cr, Prof. H. Konno (Hokkaido University, Japan) for kindly providing $NdCrO_3$ and $NdCrO_4$, as well as Prof. P. Tregenna-Piggott and C. Dobe (University of Bern, Switzerland) for providing chromous acetate. This work was supported by ONR program elements 61153N and 0602236N.

References

[1] V.M. Burns, R.G. Burns, Geochim. Cosmochim. Acta 39 (1975) 903.
[2] T.E. Bunch, E. Olsen, Geochim. Cosmochim. Acta 39 (1975) 911.
[3] S.R. Sutton, K.W. Jones, B. Gordon, M.L. Rivers, S. Bajt, J.V. Smith, Geochim. Cosmochim. Acta 57 (1993) 461.
[4] J.-P. Li, H.St.C. O'Neil, F. Seifert, J. Pet. 36 (1995) 107.
[5] B. Hanson, J.H. Jones, Am. Mineral. 83 (1998) 669.
[6] N.L. Chabot, C.B. Agee, Geochim. Cosmochim. Acta 67 (2003) 2077.
[7] J.H. Jones, H. Palme, in: R.M. Canup, K. Righter (Eds.), Origin of the Earth and Moon, University of Arizona Press, Tucson, 2000, pp. 197–216.
[8] C.W. Stowe, Econ. Geol. 89 (1994) 528.
[9] J. Robles-Camacho, M.A. Armienta, J. Geochem. Explor. 68 (2000) 167.
[10] M.E. Losi, C. Amrhein, W.T. Frankenberger Jr., Rev. Environ. Contam. Toxicol. 136 (1994) 91.
[11] D.R. Lovley, Annu. Rev. Microbiol. 47 (1993) 263.
[12] Y.-T. Wang, in: D.R. Lovley (Ed.), Environmental Microbe–Metal Interactions, ASM Press, Washington DC, 2000, pp. 225–235.
[13] S. Fendorf, B.W. Wielinga, C.M. Hansel, Int. Geol. Rev. 42 (2000) 691.
[14] K.J. Liu, J. Jiang, X. Shi, H. Gabrys, T. Walczak, H.M. Swartz, Biochem. Biophys. Res. Comm. 206 (1995) 829.
[15] C.M. Lytle, F.W. Lytle, N. Yang, J.-H. Qian, D. Hansen, A. Zayed, N. Terry, Environ. Sci. Technol. 32 (1998) 3087.
[16] B. Deng, A.T. Stone, Environ. Sci. Technol. 30 (1996) 463.
[17] B. Deng, A.T. Stone, Environ. Sci. Technol. 30 (1996) 2484.
[18] D. Banerjee, H.W. Nesbitt, Geochim. Cosmochim. Acta 63 (1999) 1671.
[19] Y. Ku, I.-L. Jung, Water Res. 35 (2001) 135.
[20] F.A. Cotton, G. Wilkinson, Advanced Inorganic Chemistry, A Comprehensive Text, Wiley, New York, 1966, pp. 818–834.
[21] M.C. Hughes, J.M. Rao, D.J. Macero, Inorg. Chim. Acta 35 (1979) L321.
[22] L. Sallans, K. Lane, R.R. Squires, B.S. Freiser, J. Am. Chem. Soc. 105 (1983) 6352.
[23] S.I. Shupack, Environ. Health Perspect. 92 (1991) 7.
[24] N.N. Greenwood, A. Earnshaw, Chemistry of the Elements, Butterworth Heinemann, Oxford, 1998, pp. 1002–1039.
[25] D.E. Kimbrough, Y. Cohen, A.M. Winer, L. Creelman, C. Mabuni, Crit. Rev. Environ. Sci. Technol. 29 (1999) 1.
[26] J. Kotas, Z. Stasicka, Environ. Pollut. 107 (2000) 263.
[27] L. Campanella, in: S. Caroli (Ed.), Element Speciation in Bioinorganic Chemistry, Wiley, New York, 1996, pp. 419–443.
[28] R.J. Bartlett, Environ. Health Perspect. 92 (1991) 17.
[29] R.K. Tandon, P.T. Crisp, J. Ellis, R.S. Baker, Talanta 31 (1984) 227.
[30] F. Brito, J. Ascanio, S. Mateo, C. Hernández, L. Araujo, P. Gili, P. Martín-Zarza, S. Domínguez, A. Mederos, Polyhedron 16 (1997) 3835.
[31] M. Cieslak-Golonka, Polyhedron 15 (1995) 3667.
[32] R. Codd, C.T. Dillon, A. Levina, P.A. Lay, Coord. Chem. Rev. 216–217 (2001) 537.
[33] C. Cervantes, J. Campos-García, S. Devars, F. Gutiérrez-Corona, H. Loza-Tavera, J.C. Torres-Guzmán, R. Moreno-Sánchez, FEMS Microbiol. Rev. 25 (2001) 335.
[34] D. Rai, B.M. Sass, D.A. Moore, Inorg. Chem. 26 (1987) 345.
[35] D. Rai, L.E. Eary, J.M. Zachara, Sci. Total Environ. 86 (1989) 15.
[36] M. Fukushima, K. Nakayasu, S. Tanaka, H. Nakamura, Anal. Chim. Acta 317 (1995) 195.
[37] R.A. Griffin, A.K. Au, R.R. Frost, J. Environ. Sci. Health A 12 (1977) 431.
[38] M. Foldesová, P. Dillinger, P. Lukác, J. Radioanaly. Nucl. Chem. 245 (2000) 435.
[39] A. Chakir, J. Bessiere, K. EL. Kacemi, B. Marouf, J. Hazard. Mater. B 95 (2002) 29.
[40] K.W. Jennette, J. Am. Chem. Soc. 104 (1982) 874.
[41] P. Arslan, M. Beltrame, A. Tomasi, Biochim. Biophys. Acta 931 (1987) 10.
[42] T. Suzuki, N. Miyata, H. Horitsu, K. Kawai, K. Takamizawa, Y. Tai, M. Okazaki, J. Bacteriol. 174 (1992) 5340.
[43] K.J. Liu, J. Jiang, H.M. Swartz, X. Shi, Arch. Biochem. Biophys. 313 (1994) 248.
[44] C.R. Myers, B.P. Carstens, W.E. Antholine, J.M. Myers, J. Appl. Microbiol. 88 (2000) 98.
[45] T.L. Kalabegishvili, N.Y. Tsibakhashvili, H.-Y.N. Holman, Environ. Sci. Technol. 37 (2003) 4678.
[46] A.L. Neal, K. Lowe, T.L. Daulton, J. Jones-Meehan, B.J. Little, Appl. Surf. Sci. 202 (2002) 150.
[47] L.S. Clesceri, A.E. Greenberg, A.D. Eaton (Eds.), Standard Methods for the Examination of Water and Wastewater, American Public Health Association, Washington, DC, 1999.
[48] J.M. Eckert, R.J. Judd, P.A. Lay, A.D. Symons, Anal. Chim. Acta 255 (1991) 31.
[49] L.A. Ellis, D.J. Roberts, J. Chromatogr. A 774 (1997) 3.
[50] F. Ahern, J.M. Eckert, N.C. Payne, K.L. Williams, Anal. Chim. Acta 175 (1985) 147.
[51] G.C. Allen, M.T. Curtis, A.J. Hooper, P.M. Tucker, J. Chem. Soc. Dalton Trans. 16 (1973) 1675.
[52] G. Cressey, C.M.B. Henderson, G. van der Laan, Phys. Chem. Miner. 20 (1993) 111.
[53] P.M. Schosseler, A.U. Gehring, Clay. Clay Miner. 44 (1996) 470.
[54] J. Chappell, B. Chiswell, A. Canning, Talanta 46 (1998) 23.
[55] J. Telser, L.A. Pardi, J. Krzystek, L.-C. Brunel, Inorg. Chem. 37 (1998) 5769.
[56] Z. Tass, G. Horvath, V.K. Josepovits, Surf. Sci. 331–333 (1995) 272.
[57] B.J. Wood, D. Virgo, Geochim. Cosmochim. Acta 53 (1989) 1277.
[58] G.J. Zhang, Y.R. Chen, R. Li, Y.Q. Jia, M.L. Liu, M.Z. Jin, Mater. Chem. Phys. 63 (2000) 178.
[59] K.M. Krishnan, Ultramicroscopy 32 (1990) 309.
[60] J.H. Paterson, O.L. Krivanek, Ultramicroscopy 32 (1990) 319.
[61] J.A. Fortner, E.C. Buck, Appl. Phys. Lett. 68 (1996) 3817.
[62] P.A. van Aken, B. Liebscher, V.J. Styrsa, Phys. Chem. Miner. 25 (1998) 323.
[63] Z.L. Wang, J. Bentley, N.D. Evans, J. Phys. Chem. B 103 (1999) 751.
[64] Z.L. Wang, J. Bentley, N.D. Evans, Micron 31 (2000) 355.
[65] U. Golla, A. Putnis, Phys. Chem. Miner. 28 (2001) 119.
[66] P.A. van Aken, V.J. Styrsa, B. Liebscher, A.B. Woodland, G.J. Redhammer, Phys. Chem. Miner. 26 (1999) 584.
[67] H. Xu, Y. Wang, J. Nucl. Mater. 265 (1999) 117.
[68] M. Colella, G.R. Lumpkin, E.R. Vance, G.W. Hong, C.J. Kim, J. Mater. Sci. Lett. 21 (2002) 1797.
[69] M. Colella, Z. Zhang, K.S. Finnie, Y. Zhang, K.L. Smith, E.J. Buck, Microsc. Microanal. 9 (Suppl. 2) (2003) 838CD.
[70] P.A. van Aken, Ber DMG, Beih Eur. J. Mineral. 7 (1995) 255.
[71] P.A. van Aken, B. Liebscher, Phys. Chem. Miner. 29 (2002) 188.
[72] T.L. Daulton, B.J. Little, K. Lowe, J. Jones-Meehan, Microsc. Microanal. 7 (2001) 470.
[73] T.L. Daulton, B.J. Little, K. Lowe, J. Jones-Meehan, J. Microbiol. Method. 50 (2002) 39.
[74] T.L. Daulton, B.J. Little, J.W. Kim, S. Newell, K. Lowe, Y. Furukawa, J. Jones-Meehan, D. Lavoie, JEOL News 37E (2002) 6.
[75] B.N. Figgis, J. Lewis, in: F.A. Cotton (Ed.), Progress in Inorganic Chemistry, Interscience, New York, 1964, pp. 37–239.
[76] J.L. Robbins, N. Edelstein, B. Spencer, J.C. Smart, J. Am. Chem. Soc. 104 (1982) 1882.
[77] H. Sitzmann, Coord. Chem. Rev. 214 (2001) 287.
[78] Y. Aoki, H. Konno, H. Tachikawa, M. Inagaki, Bull. Chem. Soc. Jpn. 73 (2000) 1197.
[79] R. Pankajavalli, C. Mallika, O.M. Sreedharan, V.S. Raghunathan, P.A. Premkumar, K.S. Nagaraja, Chem. Eng. Sci. 57 (2002) 3603.
[80] A. Fukami, K. Fukushima, N. Kohyama, in: R.H. Bennett, W.R. Bryant, M.H. Hulbert (Eds.), Microstructure of Fine-grained Sediments from Mud to Shale, Springer, New York, 1991, pp. 321–331.

[81] R.D. Leapman, L.A. Grunes, P.L. Fejes, Phys. Rev. B 26 (1982) 614.
[82] P.L. Potapov, D. Schryvers, Ultramicroscopy 99 (2004) 73.
[83] J. Zaanen, G.A. Sawatzky, Phys. Rev. B 33 (1986) 8074.
[84] P. Swift, Surf. Interface Anal. 4 (1982) 47.
[85] R.F. Egerton, Electron Energy-loss Spectroscopy in the Electron Microscope, Plenum, New York, 1996.
[86] D.H. Pearson, C.C. Ahn, B. Fultz, Phys. Rev. B 47 (1993) 8471.
[87] V. Briois, Ch. Cartier dit Moulin, Ph. Sainctavit, Ch. Brouder, A.-M. Flank, J. Am. Chem. Soc. 117 (1995) 1019.
[88] D.M. Pease, S.D. Bader, M.B. Brodsky, J.I. Budnick, T.I. Morrison, N.J. Zaluzec, Phys. Lett. 114A (1986) 491.
[89] O.L. Krivanek, J.H. Paterson, Ultramicroscopy 32 (1990) 313.
[90] S. Suzuki, M. Tomita, Jpn. J. Appl. Phys. 36 (1997) 4341.
[91] L.A.J. Garvie, A.J. Craven, R. Brydson, Am. Mineral. 79 (1994) 411.
[92] G.C. Allen, P.M. Tucker, Inorg. Chim. Acta 16 (1976) 41.
[93] K. Asami, K. Hashimoto, Corros. Sci. 17 (1977) 559.
[94] T.P. Moffat, R.M. Latanision, R.R. Ruf, Electrochim. Acta 40 (1995) 1723.
[95] D.T. Clark, D.B. Adams, Chem. Phys. Lett. 10 (1971) 121.
[96] H. Konno, H. Tachikawa, A. Furusaki, R. Furuichi, Anal. Sci. 8 (1992) 641.
[97] I. Ikemoto, K. Ishii, S. Kinoshita, H. Kuroda, M.A. Alario Franco, J.M. Thomas, J. Solid State Chem. 17 (1976) 425.

REPORT DOCUMENTATION PAGE	Form Approved OMB No. 0704-0188

PLEASE DO NOT RETURN YOUR FORM TO THE ABOVE ORGANIZATION.

1. REPORT DATE *(DD-MM-YYYY)*	2. REPORT TYPE	3. DATES COVERED *(From - To)*
08-06-2006	Journal Article (refereed)	

4. TITLE AND SUBTITLE

Determination of Chromium Valence Over the Range Cr(0)-Cr(VI) by Electron Energy Loss Spectroscopy

5a. CONTRACT NUMBER

5b. GRANT NUMBER

5c. PROGRAM ELEMENT NUMBER

PE0601153N & PE0602236N

6. AUTHOR(S)

Tyrone L. Daulton, Brenda J. Little

5d. PROJECT NUMBER

5e. TASK NUMBER

5f. WORK UNIT NUMBER

73-5052-14

7. PERFORMING ORGANIZATION NAME(S) AND ADDRESS(ES)

Naval Research Laboratory
Oceanography Division
Stennis Space Center, MS 39529-5004

8. PERFORMING ORGANIZATION REPORT NUMBER

NRL/JA/7303-05-5138

9. SPONSORING/MONITORING AGENCY NAME(S) AND ADDRESS(ES)

Office of Naval Research
800 N. Quincy St.
Arlington, VA 22217-5660

10. SPONSOR/MONITOR'S ACRONYM(S)

ONR

11. SPONSOR/MONITOR'S REPORT NUMBER(S)

12. DISTRIBUTION/AVAILABILITY STATEMENT

Approved for public release, distribution is unlimited.

13. SUPPLEMENTARY NOTES

14. ABSTRACT

Chromium is a redox active 3d transition metal with a wide range of valences (-2 to +6) that control the geochemistry & toxicity of the element. Therefore, techniques that measure Cr valence are important to bio/geochemical tools. Until now, all established methods to determine Cr valence were bulk techniques with many specific to a single, or at best, only a few oxidation state(s). We report an EELS technique along with an extensive suite of affined reference spectra that together, unlike other methods, can determine Cr valence (or at least constrain the possible valences) at high-spatial resolution (tens-of-nanometer scale) across a wide valence range, Cr(0)-Cr(VI). Fine structure of Cr-$L_{2,3}$ edges was parameterized by measurement of the chemical shift of the L3 edge & the ratio of integrated intensity under the L_3 & L_2 edges. These two parameterizations were correlated to Cr valence & also the d^n orbital configuration which has a large influence on L-edge fine structure. We demonstrate that it is not possible to unambiguously determine Cr valence from only one fine-structure parameterization which is the method employed to determine metal valence by nearly all previous EELS studies. Rather, multiple fine-structure parameterizations must be used together if the full range of possible Cr valences is considered. However, there are limitations. For example, distinguishing Cr(IV) from Cr(III) is problematic & it may be difficult to distinguish low-spin Cr(II) from Cr(III). Nevertheless, when Cr is known to be divalent, low- & high-spin d^n orbital configurations can be readily distinguished.

15. SUBJECT TERMS

Electron energy loss spectroscopy; chromium valence determination; L2,3-adsorption edges; transmission electron microscopy

16. SECURITY CLASSIFICATION OF:			17. LIMITATION OF ABSTRACT	18. NUMBER OF PAGES	19a. NAME OF RESPONSIBLE PERSON
a. REPORT	b. ABSTRACT	c. THIS PAGE			Brenda J. Little
Unclassified	Unclassified	Unclassified	UL	13	19b. TELEPHONE NUMBER *(Include area code)* (228) 688-5494